CrossMark
click for updates

View Article Online
View Journal

RSC Advances

This article can be cited before page numbers have been issued, to do this please use: R. Gupta, N. K. Eswar, J. Modak and G. Madras, *RSC Adv.*, 2016, DOI: 10.1039/C6RA16739J.

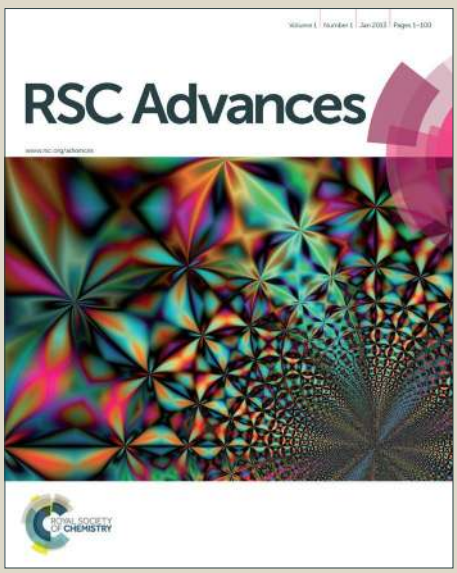

This is an *Accepted Manuscript*, which has been through the Royal Society of Chemistry peer review process and has been accepted for publication.

Accepted Manuscripts are published online shortly after acceptance, before technical editing, formatting and proof reading. Using this free service, authors can make their results available to the community, in citable form, before we publish the edited article. This *Accepted Manuscript* will be replaced by the edited, formatted and paginated article as soon as this is available.

You can find more information about *Accepted Manuscripts* in the Information for Authors.

Please note that technical editing may introduce minor changes to the text and/or graphics, which may alter content. The journal's standard Terms & Conditions and the Ethical guidelines still apply. In no event shall the Royal Society of Chemistry be held responsible for any errors or omissions in this *Accepted Manuscript* or any consequences arising from the use of any information it contains.

ROYAL SOCIETY OF CHEMISTRY

www.rsc.org/advances

Visible light driven efficient N and Cu co-doped ZnO for photoinactivation of *Escherichia coli*

View Article Online
DOI: 10.1039/C6RA16739J

Rimzhim Gupta[1], *Neerugatti KrishnaRao Eswar*[2], *Jayant M Modak*[1], *and Giridhar Madras*[1]

[1]*Department of Chemical Engineering,* [2]*Centre for Nanoscience and Engineering, Indian Institute of Science, Bangalore, India*

Published on 02 September 2016. Downloaded by New York University on 06/09/2016 11:51:34.

RSC Advances Accepted Manuscript

*Corresponding author. Tel. +91 80 22932321; Fax: +91 80 23600683,
E-mail: giridhar@chemeng.iisc.ernet.in (G. Madras)

View Article Online
DOI: 10.1039/C6RA16739J

Abstract

Co-doping of transition metal ion (Cu) and non-metal ion (N) on metal oxide substrate ZnO was achieved for the first time. The transition metal doping and N doping was carried out using combustion synthesis and hydrothermal method, respectively. Combined effect of Cu and N doping was observed by varying the Cu percentage and keeping the nitrogen doping percentage constant. The catalysts were characterized by a wide variety of techniques. Incorporation of Cu and N in ZnO matrix introduces sub energy bands near the conduction band and valence band, respectively and facilitates the absorption of longer wavelength spectra. These sub energy levels can also act as trapping sites for excitons. This results in reduced recombination and enhanced photocatalytic activity as confirmed by photoluminescence (PL). The photocatalytic inactivation of Gram negative bacteria (*E.coli*) was investigated using the N and Cu co-doped ZnO under UV and visible irradiation with different atom % of Cu. Kinetic analysis was used to obtain the order and rate constant of the inactivation reactions.

Keywords: Metal and non-metal doping; Band gap narrowing; Photocatalysis; antibacterial.

Published on 02 September 2016. Downloaded by New York University on 06/09/2016 11:51:34.

RSC Advances Accepted Manuscript

View Article Online
DOI: 10.1039/C6RA16739J

Published on 02 September 2016. Downloaded by New York University on 06/09/2016 11:51:34.

1. Introduction

Microbial contamination of water is one of the major concerns around the globe. Bacteria such as *E.coli* are major water-borne contaminants[1]. Elimination of these contaminations is a big environmental challenge. AOP[2] (advanced oxidation processes) are reported as efficient processes for mineralization of the organic impurities. Among AOP's, photocatalysis is a widely used method in the field of water purification. Therefore, development of novel nanomaterials for photocatalysis that can utilize enhanced photoredox chemistry and high surface to volume ratio is needed [3].

Metal oxides having wide energy band gap (e.g. TiO_2, ZnO, SnO_2 etc.), have been reported to demonstrate good activity for antibacterial applications[4]. However, these materials utilize only the UV region of the solar spectra. Several studies have explained the possible facilitation of visible light absorption such as narrowing the band gap either by metal, non-metal doping[5], metal / non-metal co-doping followed by embedding photo sensitizers such as CdS[6], Fe_2O_3 and other semiconductor such as Ag_3PO_4[7], AgBr[8] etc.

Transition metal and noble metal doping have been reported to improve the properties of metal oxide by generating lower energy states, facilitating electron trapping and thus decreasing the band gap. Ce[9], Ag[10], Co[11], Mn[12], Fe[13] doped ZnO have been reported for UV assisted and Cu[14], Fe[13] doped ZnO for visible light assisted for antimicrobial application. Mn and Co co-doped ZnO[15], Mg and F co-doped ZnO[16] have also been reported for antibacterial applications. N and F co-doped ZnO has been studied for inactivation of *E.coli* [17]. A recent study has been performed for F and Cu co-doped TiO_2[18]. The redox energy states of transition metals lie between the energy band gaps of semiconductor. This serves as an electron or hole trap depending upon its position with

RSC Advances Accepted Manuscript

View Article Online
DOI: 10.1039/C6RA16739J

respect to the valence or conduction band[19]. Therefore, selection of dopant from transition metals is crucial for the development of visible light active materials.

However, transition metal doping has also been reported to have certain limitations[20] such as thermal instability. Therefore, non-metals are widely preferred for band gap narrowing. Nitrogen doping into metal doped metal oxide overcomes this drawback. Mixing of N 2p and O 2p states helps in narrowing the band gap of the semiconductor and resulting in absorption of visible wavelength spectra. Thus, non-metal doping demonstrates higher photocatalysis in visible region[21]. Studies based on N doped TiO_2 have suggested the presence of nitrogen in both interstitial and substitutional sites of TiO_2 crystal[22]. Photoluminescence studies of N and Cu doped ZnO thin films have also been performed[23]. In interstitial doping, the dopant is inserted into the voids present in the lattice of the crystal structure while substitutional doping replaces the parent atom by the dopant atom. Either interstitial or substitutional doping can result in the change in electronic and optical properties of the parent material.

Non-metal doping such as C, N, S and F in TiO_2[24] are reported for various applications. Similarly, several important properties of nitrogen make it favourable to select it as a dopant. Nitrogen atoms can replace oxygen and occupy those sites[25], the comparable size of nitrogen to oxygen, small ionization energy of N than O[19, 20] are few reasons for this substitutional doping. The presence of nitrogen in the interstitial sites of metal oxide might promote the introduction of sub-bands above the valence band, as observed in N-TiO_2[26]. Band positioning of the interband in interstitial doping is higher than that of substitutional doping for TiO_2[27]. Thus electron excitation from high occupied level to conduction band is easier for interstitial doping.

Published on 02 September 2016. Downloaded by New York University on 06/09/2016 11:51:34.

RSC Advances Accepted Manuscript

View Article Online
DOI: 10.1039/C6RA16739J

Among several transition metals, Cu is incorporated in the semiconductor in the present study because of various interesting properties. First, ionization energy of Cu is higher than Zn. Secondly, low formation energy of I-B group elements facilitate the incorporation of impurity percentage in high concentration[28]. Third, large coupling between p-orbitals of oxygen and d-orbitals of impurity indicate the smaller effective mass that enhances the transport of electron in the lattice[29]. Cu doping can affect the optical properties and also modify the surface of ZnO significantly[30].

Combustion synthesis gives porous particles due to high activation energy of reactants and exothermicity of the reactions[31]. Non-metal nitrogen doping was performed by hydrothermal method[32]. This method avails homogeneously distributed "N" content by efficient transport of the reactant molecules to the active sites of the porous combustion synthesized material, expecting better efficiency of the photocatalysts[33].

The novelty in this present study is the development of transition metal and non-metal doped metal oxide i.e. N and Cu co-doped ZnO for photo-inactivation of microorganisms. The activity of Cu doped ZnO was examined for different atom percentages of Cu keeping the non-metal (N) percentage constant. Power law kinetics was used for determining the rate constants and order of bacterial inactivation.

2. Experimental section

2.1. Materials and methods

Copper nitrate trihydrate ($Cu(NO_3)_2.3H_2O$), zinc nitrate hexahydrate ($Zn(NO_3)_2.6H_2O$), glycine ($C_2H_5NO_2$), triethanolamine and potassium iodide (KI) were purchased from Merck (India). TEMPOL was purchased from Sigma-Aldrich (India). Deionized water was used for all the synthesis and experiments.

Published on 02 September 2016. Downloaded by New York University on 06/09/2016 11:51:34.

RSC Advances Accepted Manuscript

View Article Online
DOI: 10.1039/C6RA16739J

2.1.1. Photocatalysts: preparation and characterization

ZnO nanoparticles were prepared by the combustion synthesis method.[34] Zinc nitrate hexahydrate $Zn(NO_3)_2.6H_2O$ was used as precursor and glycine was used as a fuel. Stoichiometric amounts of $Zn(NO_3)_2.6H_2O$ and glycolic acid were dissolved in DI water and sonicated for 5 min separately. Later, both the solutions were mixed using sonicator for 2 min. This solution was kept in the furnace at 450 °C for 25 min that follows the following reaction.

$$9\,[Zn(NO_3)_2.6H_2O] + 10\,[NH_2CH_2COOH] \rightarrow 9\,ZnO + 20\,CO_2 + 14\,N_2 + 79\,H_2O \quad (1)$$

ZnO powder was calcined at 500 °C for 2 h in muffle furnace for removal of all impurities present in the catalyst.

Cu doping in ZnO was accomplished by the combustion method. Hereafter, 0.5, 1.5, 2.5 and 5.0 atom % Cu co-doped ZnO are denoted by Cu0.5Z, Cu1.5Z, Cu2.5Z and Cu5.0Z, respectively. In order to obtain $Cu_xZn_{(1-x)}O_{(2-\delta)}$, (x is the doping amount and δ is spill over valence of oxygen), calculated amount of doping precursor copper nitrate trihydrate ($Cu(NO_3)_2.3H_2O$), zinc nitrate hexahydrate ($Zn(NO_3)_2$).$6H_2O$ and fuel glycine (NH_2CH_2COOH) were dissolved in 15 mL of DI water and sonicated for 5 min. All the solutions were mixed and again sonicated for 2 min. The solution was kept in the furnace for 35 min at 450 °C. The recovered powder was calcined at 500 °C for 2 h in muffle furnace for complete removal of carbon impurities present in the material.

$$x\,Cu(NO_3)_2.3H_2O + (1-x)\,Zn(NO_3)_2.6H_2O + NH_2CH_2COOH \rightarrow Cu_xZn_{(1-x)}O_{(2-\delta)} + \text{gaseous products} \quad (2)$$

Published on 02 September 2016. Downloaded by New York University on 06/09/2016 11:51:34.

RSC Advances Accepted Manuscript

View Article Online
DOI: 10.1039/C6RA16739J

Nitrogen doping was carried out using the hydrothermal method. Hereafter, nitrogen doped ZnO and N and (0.5, 1.5, 2.5 and 5.0) atom % Cu co-doped ZnO are denoted by NZ, Cu0.5NZ, Cu1.5NZ, Cu2.5NZ and Cu5.0NZ, respectively. 5 mL of triethanolamine was mixed in 55 mL of DI water and sonicated for 20 min. 250 mg of Cu doped ZnO nanoparticles was dispersed using ultasonicator for 30 min in 40 mL of the amine solution. The obtained solution was transferred to Teflon reactor and fixed properly inside stainless steel autoclave. This setup was maintained at 180 °C for 22 h in muffle furnace. The obtained solution was washed with ethanol and water twice, then suspended in ethanol and kept in vacuum oven at 60 °C for drying.

Published on 02 September 2016. Downloaded by New York University on 06/09/2016 11:51:34.

2.2. Photocatalytic reactor

A batch reactor was kept on a magnetic stirrer for continuous homogeneous mixing. A quartz beaker was used for UV experiments and a glass beaker for the experiments in visible light. The lamp was covered by a quartz jacket in which a continuous supply of cold water is provided to minimize the heat dissipation from the lamp. The lamp was connected to the ballast to provide a constant power supply. For visible irradiation metal halide lamp was used (400 W) with $K_2Cr_2O_7$ UV cut-off solution filter and for UV irradiation mercury vapour lamp (150 W) was used. Lamp intensity was measured by lux meter. For UV light mercury vapour lamp intensity was 36,000 lux and for metal halide lamp, the intensity was found to be 89,000 lux.

2.3. Culture preparation and bacterial growth

The culture was prepared by inoculation of 100 µL of inoculum in 300 mL of sterilized Luria-Bertani Broth (HiMedia, India). It was kept for shaking in the incubator at 37 °C at 160 rpm for 6 h in aerobic conditions applying a cotton plug on the mouth of

RSC Advances Accepted Manuscript

View Article Online
DOI: 10.1039/C6RA16739J

conical flask. Inoculum was prepared by using glycerol stock of *E.coli* stored at -80°C. 50 µL of glycerol stock was poured in 5 mL of sterilized Luria- Bertani Broth in a centrifuge tube sealed with cotton plug. Inoculum was kept at 160 rpm at 37°C for 8-9 h such that the bacteria reaches its log growth phase. For viable count of bacteria, sterilized 2.8 % of nutrient agar (HiMedia, India) in DI water was taken as solid media for the growth of bacteria on agar plates at optimum temperature (37 °C) of bacterial growth.

Published on 02 September 2016. Downloaded by New York University on 06/09/2016 11:51:34.

2.4. Experimental procedure

30 mL of freshly prepared culture was centrifuged at 3500 rpm for 20 min. The obtained bacterial pellet was washed with sterile DI water and resuspended in 30 mL of sterile DI water along with the desired amount of catalyst. Bacterial solution was kept in dark for 1 h. The lamp was switched on and samples were collected at the interval of 20 min for 1 h. Serial dilution was accomplished 10 times with 900 µL of sterile water and 100 µL of the previous dilution. 100 µL of the diluted sample was plated on the solid agar plate for bacterial enumeration. In order to assure the reproducibility of results, the plating was done in triplicates. All the accessories used in the experiment such as glassware and micropipette tips, DI water (Millipore Milli-Q, 18 M-cm), Eppendorf tubes, centrifuge tubes were sterilized at 121°C for 90 min using autoclave.

2.5. Characterization

X-ray diffraction of the synthesized materials was analyzed by Rigaku Diffractometer at a scan rate of 1° min^{-1} from 10°- 80° with target material Cu (λ corresponding Kα emission 1.54 Å). For microscopic analysis, SEM and TEM were performed. Scanning electron microscopy was done by ULTRA55 FESEM, Carl Zeiss. For morphological analysis, SEM samples were prepared by the dispersion of catalyst in ethanol/IPA in sonicator for

RSC Advances Accepted Manuscript

View Article Online
DOI: 10.1039/C6RA16739J

10 min. The dispersed catalyst was drop-casted onto silicon wafer adhered to carbon tape and placed on aluminium stub. The samples were kept overnight under vacuum. Just before imaging, samples were sputtered with gold using Quorum sputtering. Tecnai F30 was used for transmission electron microscopy operated at 180 kV. Samples for TEM were prepared by dispersion of catalyst particles in IPA and ultrasonicated for 10 min. The dispersed catalyst was drop-casted on Cu TEM grid carefully and dried. Samples were kept in desiccator overnight to avoid undesirable interactions. In order to evaluate the reduction in band gap of the synthesized materials, diffused reflectance spectroscopy was performed using solid state UV-VIS spectrophotometer (Perkin Elmer, Lambda 35). Photoluminescence was performed by Perkin-Elmer PL instrument at excitation wavelength of 300 nm. BET surface area analysis was carried out using Nova-1000 Quantachrome.

Published on 02 September 2016. Downloaded by New York University on 06/09/2016 11:51:34.

RSC Advances Accepted Manuscript

2. Results and discussion

Nitrogen and Cu co-doped ZnO (CuxNZ, hereafter, where x is doping percentage in atom %) was synthesized successfully. Cu doped ZnO (CuxZ, hereafter, where x is doping percentage in atom %) was prepared by combustion synthesis and nitrogen doping (NZ, hereafter) was done using hydrothermal method. Cu0.5NZ, Cu1.5NZ, Cu2.5NZ, Cu5.0NZ have been used for N and (0.5, 1.5, 2.5, 5) atom % Cu co-doped ZnO.

3.1. Catalyst characterization

3.1.1. X-Ray diffraction analyses

Fig. 1(a), (b), (c), (d) and (e) represent the X-ray diffraction pattern of ZnO and different atom % of Cu doped ZnO. All the samples have hexagonal lattice structure. ZnO XRD peak positions were validated by JCPDS-00-036-1451 and CuO peak positions were validated by JCPDS-00-003-0884. The XRD pattern shows that up to 1.5 atom % Cu

View Article Online
DOI: 10.1039/C6RA16739J

doping, there was no CuO peaks observed. However, for Cu2.5NZ and Cu5.0NZ, few CuO peaks were observed that shows the presence of CuO in the synthesized materials. From the Fig. 1(a) (b) (c) (d) and (e), planes (1 0 0), (0 0 2), (1 0 1), (1 0 2), (1 1 0), (1 0 3), (1 1 2) correspond to ZnO peaks and in Fig. 1 (d) and (e), the plane (1 0 0) that corresponds to CuO peak indicates the formation of CuO in the corresponding materials at higher atom % of Cu doping (JCPDS-00-001-1117). Fig. 1 (f), (g), (h), (i) and (j) show the X-ray diffraction pattern of NZ and CuxNZ. Planes (1 0 0), (0 0 2), (1 0 1), (1 0 2), (1 1 0), (1 0 3), (1 1 2) correspond to ZnO peaks. In Fig. 1 (i) and (j), an additional peak of copper oxide (JCPDS-00-005-0667) that corresponds to plane (2 0 0) indicates the presence of Cu_2O. Copper oxide is observed as shown in fig. 1 (d), (e), (i) and (j) beyond threshold doping percentage. The formation of Cu_2O instead of CuO at higher Cu doping in Cu2.5NZ and Cu5.0NZ may be attributed to the highly alkaline envinronment created due to the presence of amines under high pressure during N doping[35]. Such phenomena of oxide formation at high concentration of doping during combustion synthesis has also been reported[36]. Slight shifting in the peak positions denotes the doping of foreign atom (Cu and N) in the lattice.

Scherrer's formula was used to determine the crystallite size obtained from the synthesized photocatalysts. The values are tabulated in Table 1. It was found that the crystallite size increases as the doping percentage was increased. Lattice parameters were also calculated for doped and co-doped photocatalysts using Rietveld refinement. The lattice parameter values are listed in Table 1. Lattice contraction and expansion depends upon the ionic radii and the concentration of the dopant[37]. At lower concentration of Cu doping, a decrease in lattice parameters was observed.

Published on 02 September 2016. Downloaded by New York University on 06/09/2016 11:51:34.

RSC Advances Accepted Manuscript

View Article Online
DOI: 10.1039/C6RA16739J

Published on 02 September 2016. Downloaded by New York University on 06/09/2016 11:51:34.

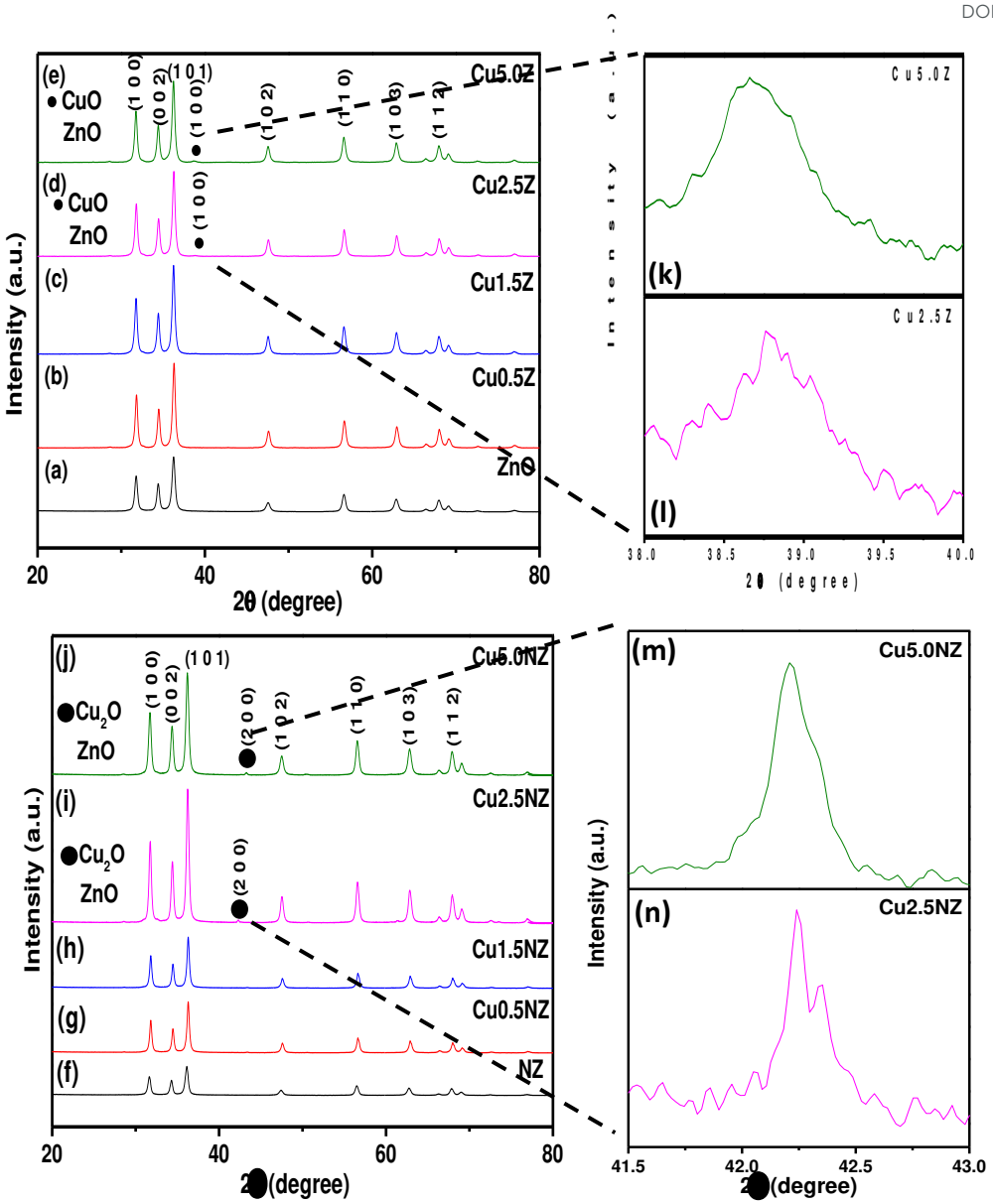

Fig. 1 X-ray diffraction pattern of (a) ZnO (b) Cu0.5Z (c) Cu1.5Z (d) Cu2.5Z (e) Cu5.0Z (f) NZ (g) Cu0.5NZ (h) Cu1.5NZ (i) Cu2.5NZ (j) Cu5.0NZ. The subfigures (k) and (l) represent higher magnification of CuO peaks in Cu2.5Z and Cu5.0Z, respectively while (m) and (n) represent higher magnification peaks of Cu_2O in Cu2.5NZ and Cu5.0NZ respectively.

RSC Advances Accepted Manuscript

View Article Online
DOI: 10.1039/C6RA16739J

Table 1 Crystallite size and lattice parameters of the synthesized catalysts

Catalysts	Crystallite size (nm)	a=b (Å)	c(Å)
ZnO	20.1	3.2503	5.2093
0.5CuZ	23.2	3.2498	5.2051
1.5CuZ	23.1	3.2488	5.2038
2.5CuZ	22.9	3.2484	5.2030
5.0CuZ	21.4	3.2485	5.2028
NZ	20.2	3.2474	5.2039
N0.5CuZ	27.0	3.2474	5.2029
Cu1.5NZ	26.9	3.2493	5.2054
Cu2.5NZ	26.5	3.2486	5.2043
Cu5.0NZ	26.3	3.2487	5.2033

The decrease in the parameters, a and c, can be attributed to substitutional doping of Cu in the host material. Since ionic radii of Cu is lesser than Zn, hence a decrease in lattice parameter was observed[38]. Same trend was observed for co-doped materials. Since doping concentration of nitrogen was kept constant, the increase in lattice parameters was compared with corresponding Cu doped ZnO. Before doping the bonding was between 3d of Zn and 2p of oxygen. However, the bonding between 3d of Cu and 2p of oxygen after the doping results in a decrease in lattice parameters.

Published on 02 September 2016. Downloaded by New York University on 06/09/2016 11:51:34.

RSC Advances Accepted Manuscript

View Article Online
DOI: 10.1039/C6RA16739J

3.1.2. Diffuse Reflectance Spectra

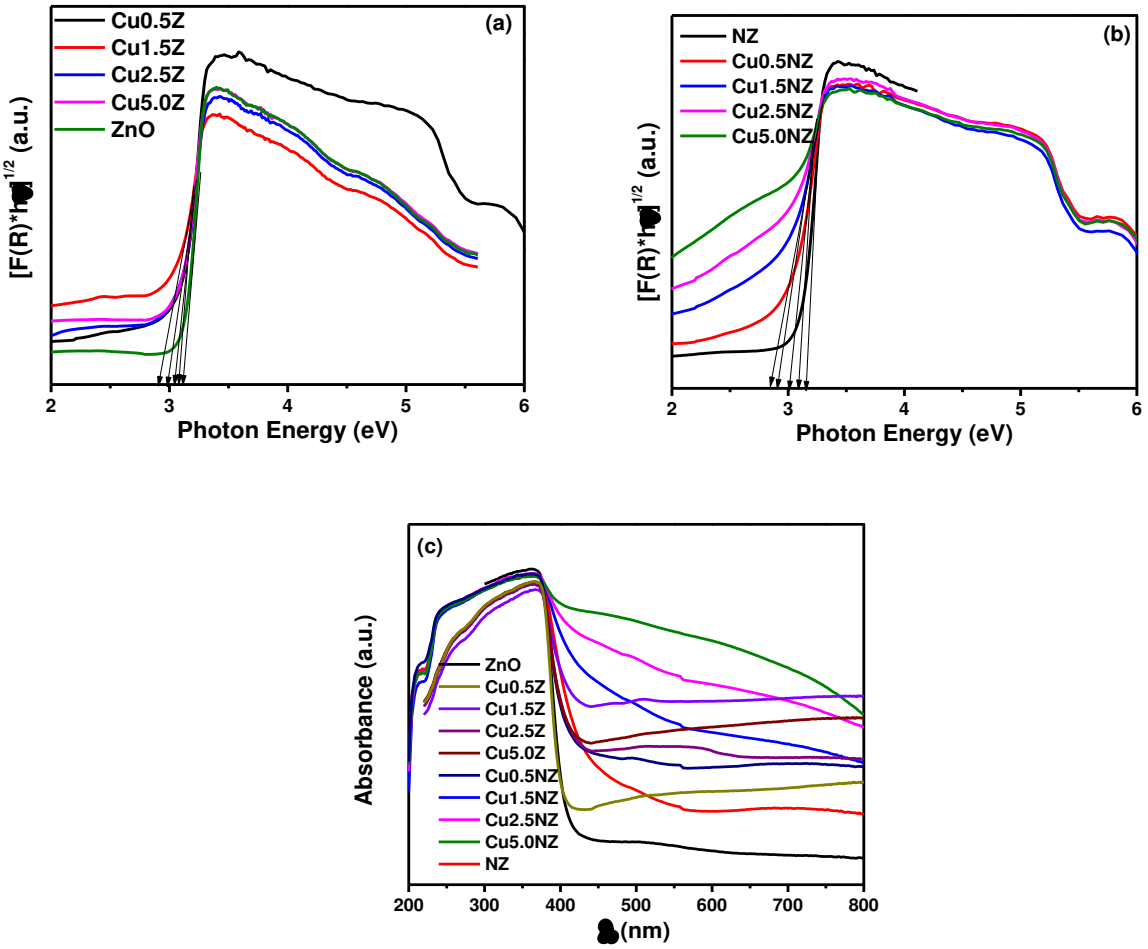

Fig. 2 (a) Band gap energy of ZnO and Cu0.5Z, Cu1.5Z, Cu2.5Z and Cu5.0Z (b) Band gap energy for NZ, Cu0.5NZ, Cu1.5NZ, Cu2.5NZ and Cu5.0NZ (c) Optical absorbance for ZnO, Cu0.5Z, Cu1.5Z, Cu2.5Z, Cu5.0Z, NZ, Cu0.5NZ, Cu1.5NZ, Cu2.5NZ and Cu5.0NZ

Fig. 2 (c) represents the absorbance of photocatalysts under UV and visible wavelength range. The UV absorbance for all the photocatalysts is similar; however, the absorption in the visible region increases as the percentage of Cu was increased. Incorporation of nitrogen in the lattice also contributes to increase the absorbance in the visible region.

Published on 02 September 2016. Downloaded by New York University on 06/09/2016 11:51:34.

RSC Advances Accepted Manuscript

View Article Online
DOI: 10.1039/C6RA16739J

It implies that on increasing the doping percentage, the optical absorbance in the visible region increases due to the reduction in band gap. The redox potential of Cu^{2+}/Cu^{0}= -4.166 eV (vacuum), lies just below the conduction band of ZnO (-4.19 eV)[19, 39].

Table 2 Band gap energy and specific surface area for all the synthesized photocatalysts

Photocatalyst	Band gap (eV)	Specific surface area (m^2/g)
ZnO	3.16	29.7
0.5CuZ	3.09	16.9
1.5CuZ	3.00	14.1
2.5CuZ	2.91	15.6
5.0CuZ	2.84	15.7
NZ	3.11	23.8
Cu0.5NZ	3.07	11.9
Cu1.5NZ	2.91	18.8
Cu2.5NZ	3.03	18.3
Cu5.0NZ	2.98	17.4

Higher the concentration of Cu, lower will be the redox potential, and lower will be the band gap. Incorporation of nitrogen also contributes in the absorption response of the photocatalyst towards visible light. In Fig. 2 (a) and (b), the band gap was calculated by the inflection point of the curve drawn between photon energy (eV) and $[\text{Kubelka Munk Function} * h\vartheta]^{1/n}$ (Tauc plot) and the calculated band gaps are tabulated in Table 2.

Published on 02 September 2016. Downloaded by New York University on 06/09/2016 11:51:34.

RSC Advances Accepted Manuscript

View Article Online
DOI: 10.1039/C6RA16739J

3.1.3. X-ray photoelectron Spectroscopy

XPS studies were conducted for better understanding of the oxidation state of the components present in photocatalyst. The elements present in the co-doped material are C, Cu, N, O and Zn. Fig. 3 (a) and (b) show the XPS spectra of C (1s) orbital. The extended peak of carbon confirms carbon bonding. Fig. 3 (c) and (d) show the wide spectra for Cu1.5NZ and ZnO respectively. Fig. 3 (e) and (f) show the XPS spectra of Zn (FWHM = 0.8 eV) (2p) orbital of undoped and co-doped ZnO the peaks correspond to $2p_{3/2}$ and $2p_{1/2}$ and the difference between the peaks is found to be 23.14 and 23.1 eV, respectively. A shift in the binding energy of Zn peaks was observed in the co-doped material [40].

The peak intensities are in the ratio of 2:1 which indicates the +2 oxidation state of Zn in ZnO. Fig. 3 (g) and (h) represent the XPS spectra for O (1s). These peaks indicate the presence of oxygen in various forms. In Fig. 3 (g) deconvoluted peaks at 531.05 eV and 531.9 eV and in Fig. 3 (h) peaks at 531.2 eV and 532 eV confirm the presence of oxygen vacancies (O_V) and chemisorbed oxygen (O_C) in both ZnO and Cu1.5NZ[41, 42]. In Fig. 3 (i), the two deconvoluted peaks at 933 eV denote the presence of Cu in the lattice in Cu^{2+} and Cu^{+} ionic form[43, 44]. The presence of the peak at 943 eV denotes the Cu^{2+} satellite in CuO, which shows the presence of Cu in ionic form. Peaks at 954 eV and 933 eV denotes $2p_{1/2}$ and $2p_{3/2}$ orbital peaks of Cu ion respectively.

Published on 02 September 2016. Downloaded by New York University on 06/09/2016 11:51:34.

RSC Advances Accepted Manuscript

View Article Online
DOI: 10.1039/C6RA16739J

Published on 02 September 2016. Downloaded by New York University on 06/09/2016 11:51:34.

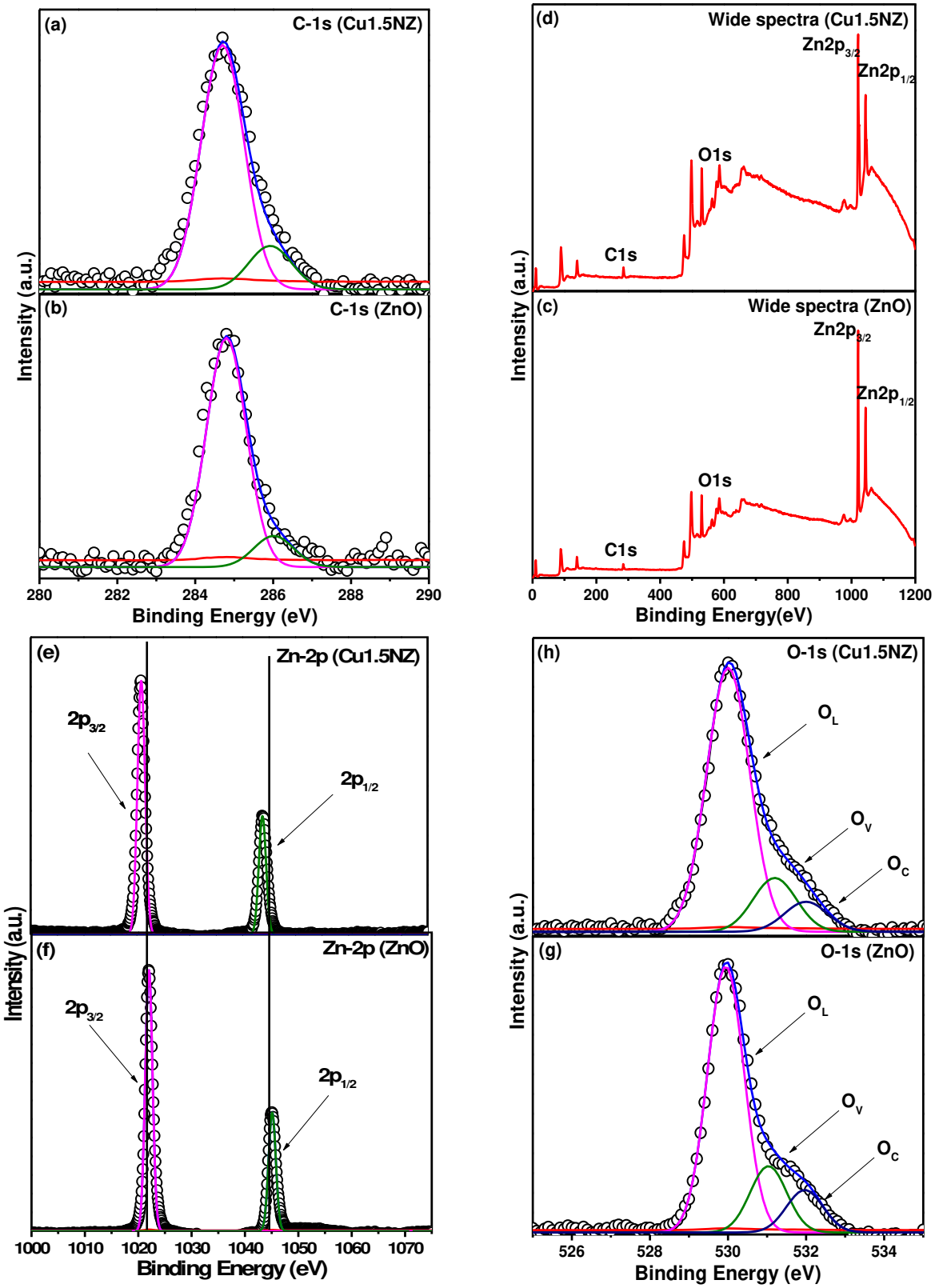

Fig. 3 XPS spectra of (a) C in Cu1.5NZ and (b) C in ZnO (c) wide spectra of Cu1.5NZ (d) wide spectra of pristine ZnO (e) Zn-2p of Cu1.5NZ and (f) Zn-2p of ZnO (g) O-1s of Cu1.5NZ and (h) O-1s of pristine ZnO

RSC Advances Accepted Manuscript

View Article Online
DOI: 10.1039/C6RA16739J

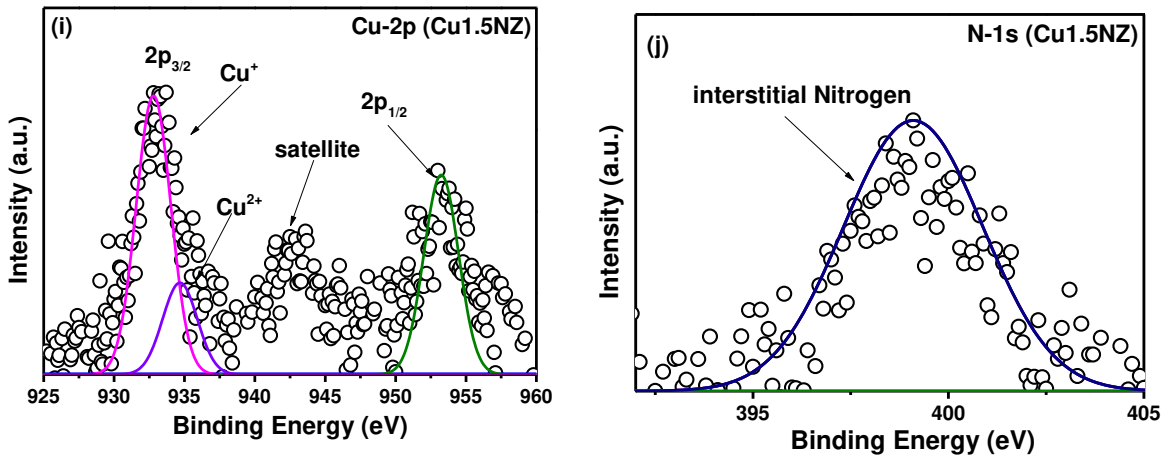

Fig. 3 XPS spectra (i) Cu in Cu1.5NZ (j) N in Cu1.5NZ.

In Fig. 3 (j), peak at 399.9 eV confirms the nitrogen presence at interstitial sites in the ZnO lattice[26]. DFT calculations from several reports show the positioning of inter-band 0.74 eV above than the valence band of TiO_2 in N doped TiO_2. The presence of nitrogen peak at 399.6 eV signifies the presence of interstitial nitrogen in NO_x or ZnN_xO form[45]. Nitrogen doping under mild conditions and in small concentration results in interstitial doping and also facilitates more oxygen vacancies[26]. Doping percentage of nitrogen was calculated based on the area under the peak and atomic sensitivity factor for corresponding element. The concentration of nitrogen on the surface of Cu1.5NZ was found to be 0.55 atom %.

3.1.4. Morphological and surface area analysis

3.1.4.1. Microscopic analysis

The morphology of the synthesized materials was determined by scanning electron microscopy. Fig. 4 (a) is the SEM image of ZnO that shows the combustion synthesized ZnO nanoparticles. Fig. 4 (b) shows Cu doped ZnO that forms a porous network of nanoparticles. In combustion synthesis, the reducer plays an important role in determining the morphology of nanoparticles. Glycine was used as a reducer for Cu doped ZnO which

Published on 02 September 2016. Downloaded by New York University on 06/09/2016 11:51:34.

RSC Advances Accepted Manuscript

View Article Online
DOI: 10.1039/C6RA16739J

has heat of combustion (-975 kJ/mol). Release of high rate of CO_2 gas results in highly porous nanoparticles[46]. Fig. 4 (c) shows nitrogen doped ZnO by the hydrothermal method that has similar morphology as that of ZnO. Fig. 4 (d) shows the dense porous network of particles due to nitrogen doping in Cu doped ZnO. Denser matrix is the result of interstitial doping of nitrogen. Nitrogen doping modifies the surface structure of the parent material[19]. This results in the loose packing forming pores visible in Fig. 4 (a) and (b).

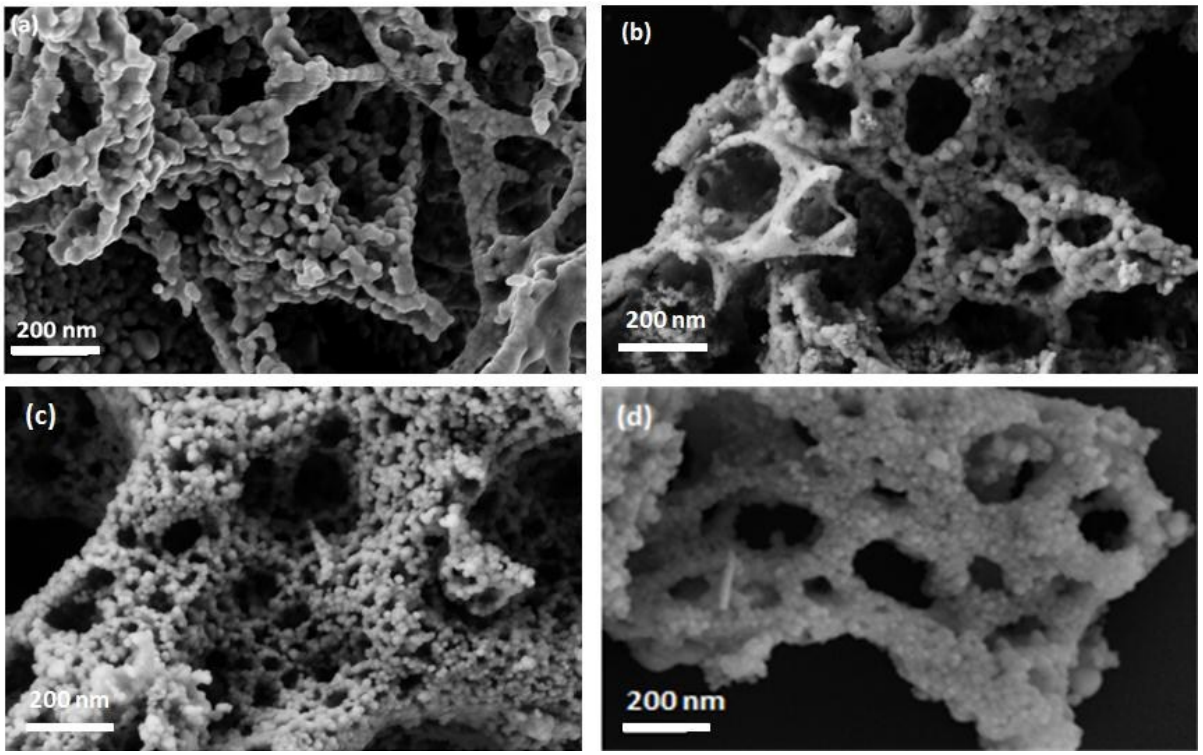

Fig. 4 SEM images of (a) ZnO (b) Cu1.5Z (c) NZ (d) Cu1.5NZ

Fig. 5 (a) and (b) shows the high resolution TEM images of ZnO and N and 1.5 atom % Cu co-doped ZnO. The fringes indicate the crystallinity of the catalysts. The d-spacing is 2.528 Å and 2.501 Å ZnO and for Cu1.5NZ, respectively. Reduction in lattice d- spacing denotes the occurrence of doping and contraction in the lattice.

Published on 02 September 2016. Downloaded by New York University on 06/09/2016 11:51:34.

RSC Advances Accepted Manuscript

View Article Online
DOI: 10.1039/C6RA16739J

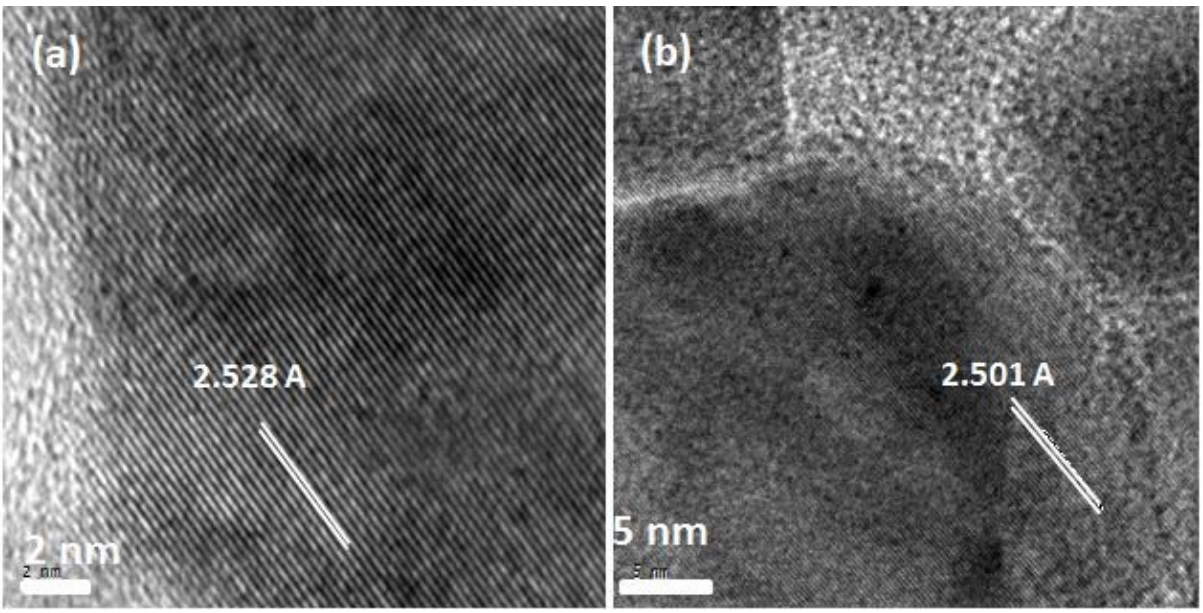

Fig. 5 HRTEM images of (a) ZnO (b) Cu1.5NZ

3.1.4.2. Bruauer-Emmett-Teller surface area analyses

Determination of the surface areas for all the prepared photocatalysts was performed. The doping incorporates strain in the grain boundaries of the crystal. The specific surface area values for all the catalysts are listed in Table 2. Table 1 shows an increase in crystallite size as doping concentration was increased. Several studies suggest that increase in crystallite size results in the reduction in specific surface area[47]. The presence of nitrogen in N_3^- form induces a charge in the particle that tends to agglomeration. This results in reduction in surface area after nitrogen doping.

Published on 02 September 2016. Downloaded by New York University on 06/09/2016 11:51:34.

RSC Advances Accepted Manuscript

View Article Online
DOI: 10.1039/C6RA16739J

3.1.5. Photoluminescence

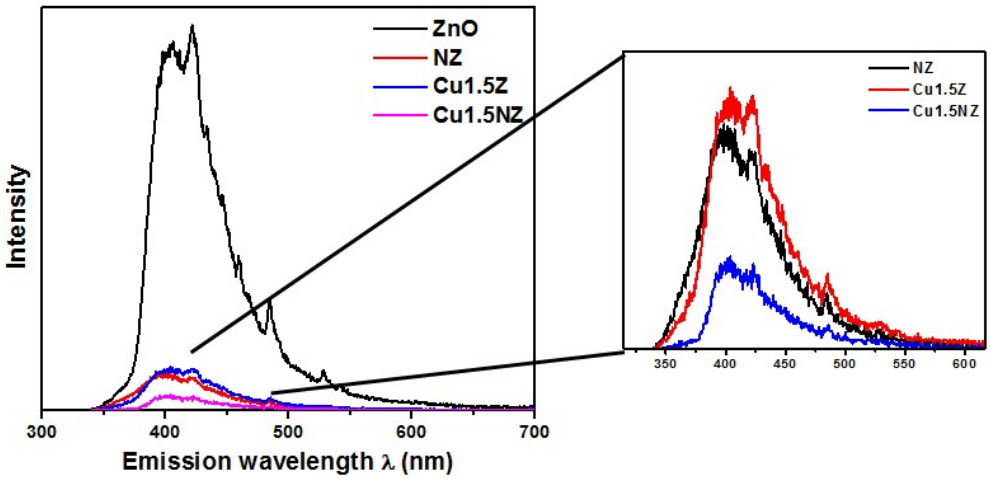

Fig. 6 Photoluminescence spectra for ZnO, NZ, Cu1.5Z, Cu1.5NZ

Fig. 6 represents the photoluminescence (PL) spectra of ZnO, N doped ZnO, 1.5 atom % Cu doped ZnO, N and 1.5 atom % Cu doped ZnO. PL spectra depict the exciton recombination. A significant intensity difference was observed between undoped ZnO and doped ZnO materials. The decreased intensity denotes the longer charge separation, and efficient charge transport without recombination. The peaks that correspond to 400-410 nm signifies the recombination of the charge carriers present at the band edges. Other weak shoulder peaks present in the range of 420-460 nm may correspond to the recombination of shallow trapped electrons and holes (450, 475, 530 nm). XPS studies showed the generation of oxygen vacancies as a result of doping. The shoulder emission peaks in all the photocatalysts at 475 nm may correspond to oxygen vacancies. Excited electrons on the conduction bands are bound at different sub-levels generated because of oxygen vacancies. These states act as recombination centres for holes and electrons[48] and results in a PL signal[49]. The recombination of excitons due to the presence of surface

Published on 02 September 2016. Downloaded by New York University on 06/09/2016 11:51:34.

RSC Advances Accepted Manuscript

View Article Online
DOI: 10.1039/C6RA16739J

defects generated after metal and non-metal doping. The shoulder peaks in ZnO at 530 nm corresponds to deep traps present at interstitial acceptor.

3.2. Photocatalysis

In order to obtain the photocatalytic activity of nitrogen and copper doped ZnO for degradation of bacteria, the experiments were carried out under visible and UV irradiation. Cu doped ZnO of different atom % (0.5, 1.5, 2.5, 5.0) was prepared by combustion synthesis and N doping was done by using hydrothermal method on Cu doped ZnO. Reaction was shown to be followed power law kinetics. In case of UV, order of reaction was found to be 1.15[50] and in visible irradiation, pseudo first order reaction was followed[51].

3.2.1. Effect of catalyst loading

In order to determine the optimum catalyst loading, experiments were carried out for catalyst loading of 0.1, 0.25, and 0.5 g/L. On increasing the loading up to 0.25 g/L, the rate of reaction increases, after that it starts decreasing. In case of 0.1 g/L, due to insufficient amount of catalyst, the optimum interaction between the catalyst and bacteria cannot be achieved. However, in case of 0.5 g/L catalyst loading, the catalysts agglomerate due to high surface energy of the particles and results in the turbidity of bacterial solution. Turbidity hinders the light to enter and allow maximum scattering of light. Same trend of inactivation is shown in other reports[52]. Fig. 7 shows the degradation profile for different catalyst loadings. Experiments were carried out in visible light with initial concentration ~10^7CFU/mL. The inset of Fig. 7 shows the trend of rate constants followed at different loadings.

Published on 02 September 2016. Downloaded by New York University on 06/09/2016 11:51:34.

RSC Advances Accepted Manuscript

View Article Online
DOI: 10.1039/C6RA16739J

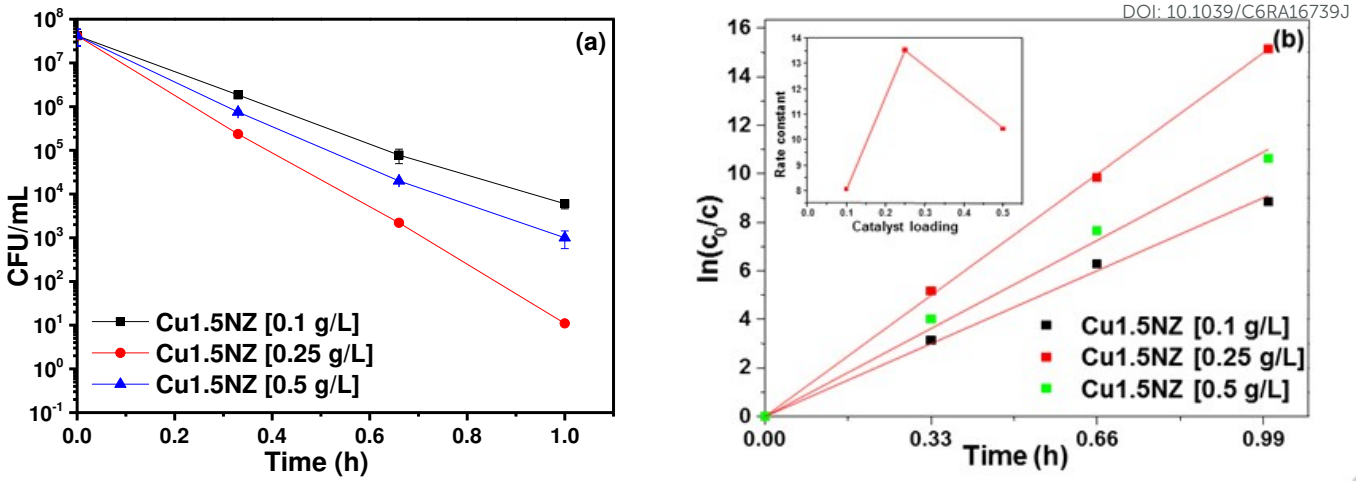

Fig. 7 (a) Degradation profile for Cu1.5NZ with initial cell concentration ~10^7-10^8 CFU/mL at catalyst loading of 0.1 g/L, 0.25 g/L and 0.5 g/L (b) Kinetics for catalyst loading of 0.1 g/L, 0.25 g/L and 0.5 g/L Cu1.5NZ (inset). Rate constants for catalyst loading of 0.1, 0.25 and 0.5 g/L

3.2.2. Catalytic effect of different catalysts

The degradation profile of *E.coli* under visible and UV irradiation for different photocatalysts are shown in Fig. 8 (a) to (d). The rate constants on the basis of followed inactivation reaction order were determined and tabulated in Table 3. The kinetics for different photocatalysts is discussed in the following sections.

3.2.2.1. Effect of Cu doping under UV light

Under UV irradiation, a gradual increase in rate constant was achieved as the doping percentage of Cu was increased from 0.5 to 1.5 atom %, due to increase in defect sites and electron trap sites, which increases the charge separation[53]. However, this happens up to an optimum doping percentage. Further increase in doping percentage results in a reduced photocatalytic activity due to formation of its corresponding oxide supported by

Published on 02 September 2016. Downloaded by New York University on 06/09/2016 11:51:34.

RSC Advances Accepted Manuscript

View Article Online
DOI: 10.1039/C6RA16739J

XRD analysis (section 3.1.1). The reduced band gap beyond 1.5 atom %, provides an ease of electron-hole recombination[54], which is supported by PL results (section 3.1.5). Trapped electrons either react with electron acceptor species and form super oxide radicals or it may recombine with hole depending upon the most favourable condition. This enhances the recombination and thus reduces the photocatalytic activity of the photocatalyst. Dopant concentrations beyond optimum give rise to high surface barriers. This leads to narrowing of the space charge and an efficient charge separation can be obtained. However, dopant concentration beyond optimum decrease the space region width of the depletion region. This results in an increased recombination. Light penetration through ZnO becomes higher than the width of space charge layer that results in easier recombination of photogenerated electrons and holes[55-57].

Fig. 8 (a) shows the degradation profile of *E.coli* for photolysis, ZnO, 0.5, 1.5, 2.5, and 5.0 atom % Cu doped ZnO in UV and visible light, respectively. The order followed by UV light inactivation is 1.15. The photocatalytic activity of Cu1.5Z showed superior results. The order of photocatalytic activity obtained under UV radiation is ZnO < Cu0.5Z < Cu5.0Z < Cu2.5Z < Cu1.5Z.

3.2.2.2. Effect of Cu doping under visible light

A similar trend was observed in the visible light exposure to the bacteria in the presence of different doping concentration of Cu on ZnO[58, 59]. As shown in Table 3, increase in doping percentage results in the decrease in the band gap of the photocatalyst. Lower band gap facilitates the absorption of longer wavelength light i.e. visible light. The gradual increase in the rate constants is the result of the lower band gap of the material i.e. absorption of visible light. Formation of inter bands nearby conduction band is the

Published on 02 September 2016. Downloaded by New York University on 06/09/2016 11:51:34.

RSC Advances Accepted Manuscript

View Article Online
DOI: 10.1039/C6RA16739J

reason of lower band gap of the photocatalyst[60]. The redox potential of copper (0.52 eV) lies between the band edges of ZnO (V.B. = 2.89 eV, C.B. = -0.31 eV). This is the major cause of the introduction of the sub-band below conduction band. No significant difference in photoactivity was observed after a threshold doping concentration (section 3.2.2.1). Fig. 8 (b) shows the degradation profile of for *E. coli* under visible light exposure. First order kinetics was observed for the inactivation reaction of *E.coli* under visible irradiation, which is shown in Fig. 8 (f). The order of photocatalytic activity for visible light is ZnO<Cu0.5Z<Cu5.0Z<Cu1.5Z<= (≈) Cu2.5Z.

3.2.2.3. Effect of N and Cu co-doping

In order to observe the effect of nitrogen doping on ZnO, experiments were carried out with constant nitrogen doping under UV and visible irradiation. Incorporation of nitrogen was in the interstitial sites in the lattice, as confirmed by XPS results[61]. After gaining the energy equivalent to the band gap, the excited electrons transfer from top of the valence band to bottom of the conduction band. Generation of oxygen vacancy creates unpaired electrons and Zn^{2+} centres that cause the introduction of other donor levels. Oxygen vacancies directly relate with the recombination of hole and electrons because it changes the transfer rate of excitons[62]. The interstitial doping of nitrogen promotes the generation of oxygen vacancies. It was reported that low doping concentration of nitrogen reduces the formation energy of oxygen vacancies[61]. This results in trapping of the excited electrons in the sub-levels related to oxygen vacancies[26]. Larger the number of oxygen vacancies will result in higher charge separation. Incorporation of N in the lattice introduces N 2p states along with already present O 2p states. This creates sub-bands nearby valence band of the ZnO which act as hole trap sites[48]. The co-doping effect is successful in other studies and applications as well[63]. Cu acts as a donor species and

Published on 02 September 2016. Downloaded by New York University on 06/09/2016 11:51:34.

RSC Advances Accepted Manuscript

View Article Online
DOI: 10.1039/C6RA16739J

nitrogen as acceptor. Presence of donor and acceptor at neighbouring sites and second neighbouring site is preferable due to high electrostatic interaction between them[64]. Presence of donor adjacent to the acceptor species reduces the energy level of acceptor. There is a level near the valence band of the semiconductor[65]. This is the reason for the enhanced photocatalytic activity under visible light. The trapping of holes and electrons by N and Cu co-doping reduces the recombination. Therefore, a gradual increase in the photoactivity can be observed from 0.5-1.5 atom % CuNZ. The subsequent reduction in the photoactivity from 1.5-5 % CuNZ is the result of narrowing of the band gap beyond optimum. Charge carrier separation and less recombination result in high photocatalytic activity.

Table 3. Rate constants of inactivation reactions under UV and visible light

Photocatalyst	**Order (n)**	**Rate constant (k) UV [Conc$^{(1-n)}$time(h^{-1})]**	**Order (n)**	**Rate constant (k) Visible [h^{-1}]**
Photolysis	1.15	0.809	1	5.38 ± 0.1
ZnO	1.15	1.014	1	7.02 ± 0.1
0.5CuZ	1.15	1.111	1	8.35 ± 0.2
1.5CuZ	1.15	1.258	1	8.96 ± 0.1
2.5CuZ	1.15	1.163	1	8.90 ± 0.2
5.0CuZ	1.15	1.061	1	7.67 ± 0.2
NZ	1	10.18 ± 0.1	1	12.08 ± 0.1
Cu0.5NZ	1	11.63 ± 0.5	1	12.58 ± 0.2
Cu1.5NZ	1	16.69 ± 0.6	1	17.68 ± 0.3
Cu2.5NZ	1	14.99 ± 0.7	1	15.90 ± 0.2
Cu5.0NZ	1	13.37 ± 0.4	1	15.12 ± 0.1

Published on 02 September 2016. Downloaded by New York University on 06/09/2016 11:51:34.

RSC Advances Accepted Manuscript

View Article Online
DOI: 10.1039/C6RA16739J

Published on 02 September 2016. Downloaded by New York University on 06/09/2016 11:51:34.

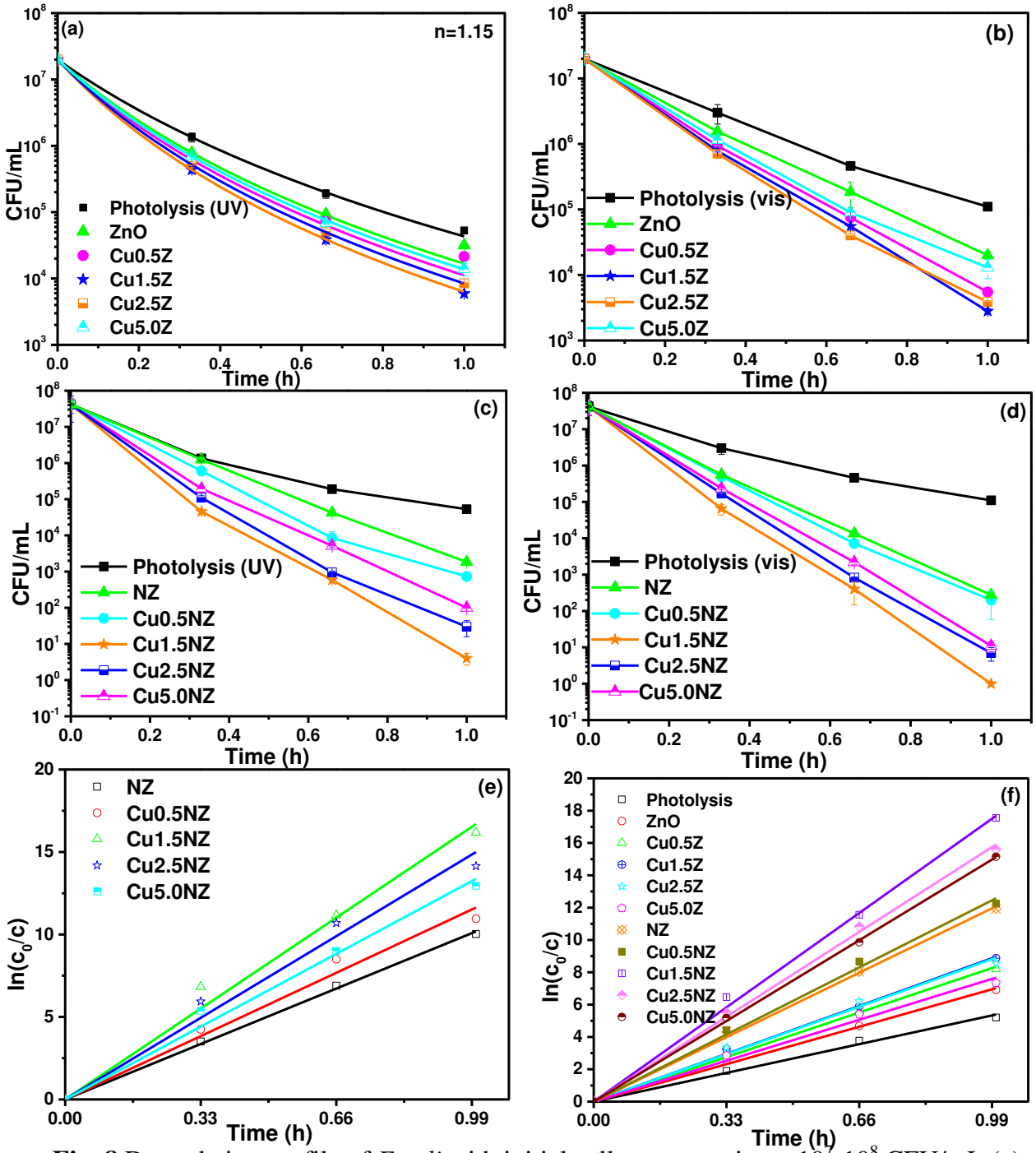

Fig. 8 Degradation profile of *E.coli* with initial cell concentration ~10^7-10^8 CFU/mL (a) Photolysis, ZnO, Cu0.5Z, Cu1.5Z, Cu2.5Z and Cu5.0Z under UV light (b) Photolysis, ZnO, Cu0.5Z, Cu1.5Z, Cu2.5Z and Cu5.0Z under visible light (c) PL, NZ, Cu0.5NZ, Cu1.5NZ, Cu2.5NZ and Cu5.0NZ under UV light (d) Photolysis, NZ, Cu0.5NZ, Cu1.5NZ, Cu2.5NZ and Cu5.0NZ under visible light (e) kinetics for N and Cu co-doped ZnO in UV light (f) kinetics for all the materials in visible light

RSC Advances Accepted Manuscript

View Article Online
DOI: 10.1039/C6RA16739J

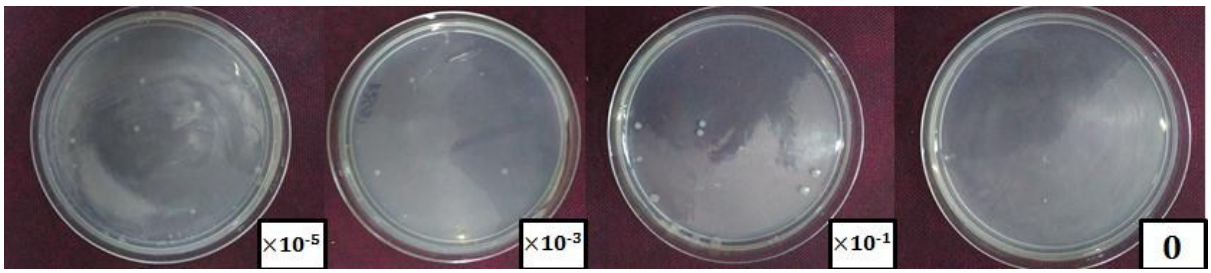

Fig. 9 Photographs of the *E. coli* colonies in the antibacterial experiment with Cu1.5NZ

Fig. 8 (c) and (d) show the inactivation of *E.coli* under UV and visible light for metal non-metal co-doped metal oxides. First order of inactivation reaction was observed. The photocatalytic activity obtained under UV and visible light irradiation follows NZ<Cu0.5NZ< N5.0Cu Z<Cu2.5NZ<Cu1.5NZ order. The kinetics of the degradation are shown in Fig. 8 (e) and (f). The rate constants and order for all the inactivation reactions are tabulated in Table 3.

Fig. 9 shows the photographs of plates count experiment carried out with 0.25 g/L of Cu1.5NZ for enumeration of bacterial colonies. 50 µL of the serially diluted sample was spread over agar plates. 8-log reduction in bacterial concentration was obtained in 1 hour.

Published on 02 September 2016. Downloaded by New York University on 06/09/2016 11:51:34.

RSC Advances Accepted Manuscript

View Article Online
DOI: 10.1039/C6RA16739J

3.2.2.4. Effect of scavenger on the bacterial concentration

To understand the major oxidative species ($\dot{O}H, \dot{O}_2^-$) responsible for the bacterial inactivation, the experiments were carried out using KI as scavenger for hydroxyl radical and 4-Hydroxy-2,2,6,6-tetramethylpiperidinyloxy (TEMPOL) as scavenger for superoxide radical[66]. Figure 10 shows the degradation profile of *E.coli* in the presence of KI and TEMPOL as scavengers. Initially, 5 mmol/L KI and 2 mmol/L TEMPOL were used without catalyst as control. It was observed that there is no significant reduction in bacterial concentration in the absence of catalyst. Experiments were also carried out in the presence of KI and TEMPOL with 0.25 g/L of catalyst (Cu1.5NZ). A comparatively large reduction in the antibacterial activity of catalyst was observed with TEMPOL addition. A small reduction in the antibacterial activity was observed when used with KI as scavenger. Thus, $\dot{O}_2^-$ radical can be considered as the major responsible species for the inactivation of bacteria in this system.

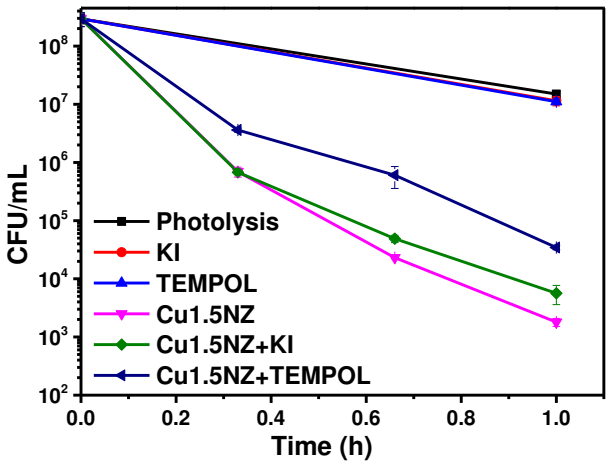

Fig. 10. Inactivation of *E. coli* by Cu1.5NZ with initial cell concentration $\sim 2 \times 10^8$ CFU/mL in the presence of KI ($(\dot{O}H)$ scavenger) and TEMPOL ($(\dot{O}_2^-)$ scavenger)

Published on 02 September 2016. Downloaded by New York University on 06/09/2016 11:51:34.

RSC Advances Accepted Manuscript

View Article Online
DOI: 10.1039/C6RA16739J

3.3. Photocatalysis Mechanism

Doping induces modifications in the electronic band structure of substrate photocatalysts[14, 21, 25, 67]. These electronic changes remove the limitation of confined usage of photocatalysts in UV light. Transition metal ion doping introduces a sub-energy level below the conduction band and nitrogen doping does the same by introducing an additional energy level just above the valence band of the metal oxide semiconductor. These sublevels act as traps for the electrons and holes generated after the exposure of the photocatalyst in photon energy higher or equal to the band gap of semiconductor. The photo excited electrons can either recombine i.e. dissipate energy in the form of heat or can be involved in redox reaction with the adsorbed species[68]. Sub-bands/intermediate bands increase the charge separation by transferring photo-excited excitons from conduction band and valence band to their meta-stable states i.e. levels generated through incorporation of impurity. If charge separation is maintained, the electrons and holes are promoted from the surface to the formation of reactive oxygen species (ROS)[68].

Mechanism of ROS generation can be understood by the schematic in Fig. 11. Excess doping concentration of transition metal may reduce the photodegradation efficiency of the photocatalysts because they could act as recombination centres and accelerate the recombination of electron and hole as the concentration increases[69]. N doping into ZnO benefits the photocatalyst by forming a p-type semiconductor. Fig. 11 shows the mechanism of the semiconductor material in pictorial form.

Published on 02 September 2016. Downloaded by New York University on 06/09/2016 11:51:34.

RSC Advances Accepted Manuscript

View Article Online
DOI: 10.1039/C6RA16739J

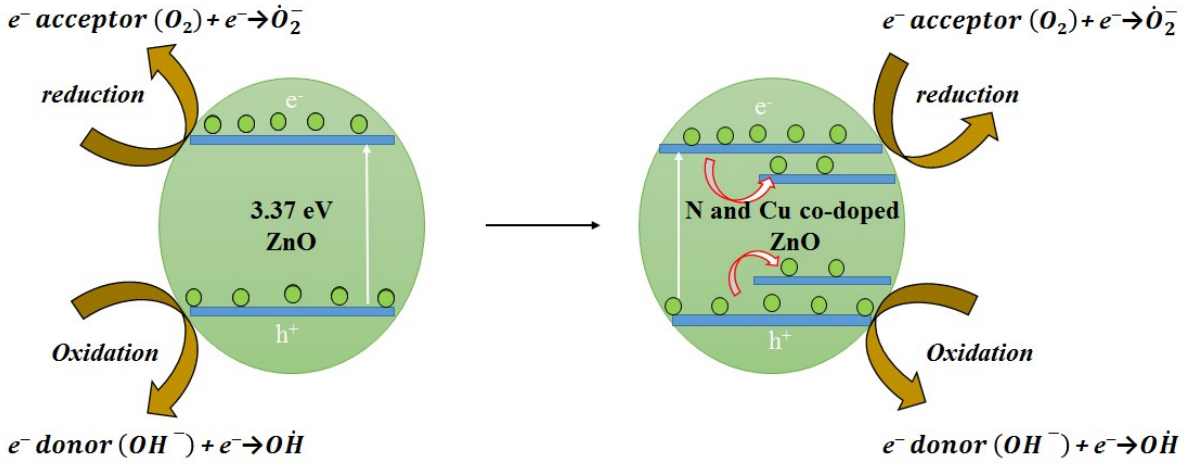

Fig. 11 Schematic of band gap changes in the photocatalyst after doping. ZnO is primarily active in the UV region while N and Cu co-doped ZnO is active in the visible light.

Published on 02 September 2016. Downloaded by New York University on 06/09/2016 11:51:34.

RSC Advances Accepted Manuscript

View Article Online
DOI: 10.1039/C6RA16739J

Conclusions

N and Cu co-doped ZnO with different Cu atom % were synthesized by combustion synthesis followed by hydrothermal method for antibacterial applications. These dopants were chosen based on strong 3d and 2p bonding between Cu and O and comparative atomic radii of N and O. Incorporation of Cu and N induces an increased charge separation and thus results in enhanced photocatalytic activity. The photocatalytic activity of N and Cu co-doped ZnO was investigated to determine the threshold doping percentage of Cu. Augmented optical absorbance resulted from narrowing of band gap by metal and non-metal doping, which is validated by diffused reflectance studies. Synergistic effects of photoactivity were achieved with the novel co-doped photocatalyst. Enhanced catalytic activity was achieved under both UV and visible light i.e. solar light. XPS studies confirm the nitrogen presence at the interstitial sites of oxygen which indicates the interstitial doping of nitrogen. This photocatalyst is a highly efficient material for photoinactivation of *E.coli* due to copper doping and interstitial nitrogen doping.

Acknowledgements

The authors are thankful to Department of Science and Technology (DST), India for the financial support, CeNSE and AFMM for characterization facilities. Giridhar Madras thanks DST for the J.C. Bose fellowship. The authors thank Dr. Archana Charanpahari for assisting in DRS and PL analysis.

Published on 02 September 2016. Downloaded by New York University on 06/09/2016 11:51:34.

RSC Advances Accepted Manuscript

View Article Online
DOI: 10.1039/C6RA16739J

References

1. H. A. Foster, I. B. Ditta, S. Varghese and A. Steele, *Applied microbiology and biotechnology*, 2011, **90**, 1847-1868.
2. R. Andreozzi, V. Caprio, A. Insola and R. Marotta, *Catalysis today*, 1999, **53**, 51-59.
3. D. Beydoun, R. Amal, G. Low and S. McEvoy, *Journal of Nanoparticle Research*, 1999, **1**, 439-458.
4. K. Kabra, R. Chaudhary and R. L. Sawhney, *Industrial & engineering chemistry research*, 2004, **43**, 7683-7696.
5. J. Zhang, Y. Wu, M. Xing, S. A. K. Leghari and S. Sajjad, *Energy & Environmental Science*, 2010, **3**, 715-726.
6. M. Zirak, O. Akhavan, O. Moradlou, Y. Nien and A. Moshfegh, *Journal of Alloys and Compounds*, 2014, **590**, 507-513.
7. N. K. Eswar, P. C. Ramamurthy and G. Madras, *Photochemical & Photobiological Sciences*, 2015, **14**, 1227-1237.
8. N. K. Eswar, V. V. Katkar, P. C. Ramamurthy and G. Madras, *Industrial & Engineering Chemistry Research*, 2015, **54**, 8031-8042.
9. C. Karunakaran, P. Gomathisankar and G. Manikandan, *Materials Chemistry and Physics*, 2010, **123**, 585-594.
10. P. Amornpitoksuk, S. Suwanboon, S. Sangkanu, A. Sukhoom, N. Muensit and J. Baltrusaitis, *Powder Technology*, 2012, **219**, 158-164.
11. R. K. Dutta, P. K. Sharma, R. Bhargava, N. Kumar and A. C. Pandey, *The Journal of Physical Chemistry B*, 2010, **114**, 5594-5599.
12. K. Rekha, M. Nirmala, M. G. Nair and A. Anukaliani, *Physica B: Condensed Matter*, 2010, **405**, 3180-3185.
13. M. Li, S. Pokhrel, X. Jin, L. Mädler, R. Damoiseaux and E. M. V. Hoek, *Environmental Science & Technology*, 2011, **45**, 755-761.
14. R. Kumar, S. Anandan, K. Hembram and T. Narasinga Rao, *ACS Applied Materials & Interfaces*, 2014, **6**, 13138-13148.
15. M. Nirmala and A. Anukaliani, *Materials Letters*, 2011, **65**, 2645-2648.
16. S. Snega, K. Ravichandran, N. Jabena Begum and K. Thirumurugan, *J Material Science: Materials in Electronics*, 2013, **24**, 135-141.
17. K. Pathakoti, S. Morrow, C. Han, M. Pelaez, X. He, D. D. Dionysiou and H.-M. Hwang, *Environmental Science & Technology*, 2013, **47**, 9988-9996.
18. N. S. Leyland, J. Podporska-Carroll, J. Browne, S. J. Hinder, B. Quilty and S. C. Pillai, *Scientific Reports*, 2016, **6,** 24770.
19. L. G. Devi and R. Kavitha, *Applied Catalysis B: Environmental*, 2013, **140**, 559-587.
20. G. Liu, L. Wang, H. G. Yang, H.-M. Cheng and G. Q. M. Lu, *Journal of Materials Chemistry*, 2010, **20**, 831-843.
21. R. Jaiswal, N. Patel, D. Kothari and A. Miotello, *Applied Catalysis B: Environmental*, 2012, **126**, 47-54.
22. R. Asahi and T. Morikawa, *Chemical Physics*, 2007, **339**, 57-63.
23. M. Liton, K. Khan, M. Rahman and M. Islam, *Journal of Scientific Research*, 2015, **7**, 23-34.
24. M. Pelaez, N. T. Nolan, S. C. Pillai, M. K. Seery, P. Falaras, A. G. Kontos, P. S. M. Dunlop, J. W. J. Hamilton, J. A. Byrne, K. O'Shea, M. H. Entezari and D. D. Dionysiou, *Applied Catalysis B: Environmental*, 2012, **125**, 331-349.
25. S. Rehman, R. Ullah, A. Butt and N. Gohar, *Journal of Hazardous Materials*, 2009, **170**, 560-569.
26. C. W. Dunnill and I. P. Parkin, *Dalton Transactions*, 2011, **40**, 1635-1640.

Published on 02 September 2016. Downloaded by New York University on 06/09/2016 11:51:34.

RSC Advances Accepted Manuscript

View Article Online
DOI: 10.1039/C6RA16739J

27. F. Peng, L. Cai, H. Yu, H. Wang and J. Yang, *Journal of Solid State Chemistry*, 2008, **181**, 130-136.
28. C. S. Chen, X. D. Xie, T. G. Liu, L. W. Lin, J. C. Kuang, X. L. Xie, L. J. Lu and S. Y. Cao, *Journal of Nanoparticle Research*, 2012, **14**, 1-8.
29. Y. Yan, M. Al-Jassim and S.-H. Wei, *Applied physics letters*, 2006, **89**, 1912.
30. M. Ahmad, E. Ahmed, Z. L. Hong, X. L. Jiao, T. Abbas and N. R. Khalid, *Applied Surface Science*, 2013, **285, Part B**, 702-712.
31. K. Nagaveni, G. Sivalingam, M. S. Hegde and G. Madras, *Applied Catalysis B: Environmental*, 2004, **48**, 83-93.
32. J. Liu, R. Han, Y. Zhao, H. Wang, W. Lu, T. Yu and Y. Zhang, *The Journal of Physical Chemistry C*, 2011, **115**, 4507-4515.
33. W. Ho, J. C. Yu and S. Lee, *Chemical Communications*, 2006, **10**, 1115-1117.
34. M. S. Hegde, G. Madras, K.C. Patil, *Accounts of Chemical Research*, 2009, **42**, 704-712.
35. Zheng, Jin You et al., *RSC Adv.*, 2014, **4** ,18616-18620.
36. K. Nagaveni, M. S. Hegde and G. Madras, *The Journal of Physical Chemistry B*, 2004, **108**, 20204-20212.
37. M. Leszczyński, E. Litwin-Staszewska, T. Suski, J. Bąk-Misiuk and J. Domagała, *Acta Physica Polonica A*, 1995, **88**, 837-840.
38. O. Lupan, T. Pauporté, B. Viana and P. Aschehoug, *Electrochimica Acta*, 2011, **56**, 10543-10549.
39. Y. Xu and M. A. Schoonen, *American Mineralogist*, 2000, **85**, 543-556.
40. A. Sasahara and M. Tomitori, *The Journal of Physical Chemistry C*, 2013, **117**, 17680-17686.
41. N. K. Eswar, P. C. Ramamurthy and G. Madras, *New Journal of Chemistry*, 2015, **39**, 6040-6051.
42. A. Leelavathi, G. Madras and N. Ravishankar, *Physical Chemistry Chemical Physics*, 2013, **15**, 10795-10802.
43. M. Kuang, T. T. Li, H. Chen, S. M. Zhang, L. L. Zhang and Y. X. Zhang, *Nanotechnology*, 2015, **26**, 304002.
44. M. C. Biesinger, L. W. M. Lau, A. R. Gerson and R. S. C. Smart, *Applied Surface Science*, 2010, **257**, 887-898.
45. A. V. Emeline, V. N. Kuznetsov, V. K. Rybchuk and N. Serpone, *International Journal of Photoenergy*, 2008, **2008**, Article ID: 258394.
46. S. T. Aruna and A. S. Mukasyan, *Current Opinion in Solid State and Materials Science*, 2008, **12**, 44-50.
47. C. Bueno-Ferrer, S. Parres-Esclapez, D. Lozano-Castelló and A. Bueno-López, *Journal of Rare Earths*, 2010, **28**, 647-653.
48. H. Irie, Y. Watanabe and K. Hashimoto, *The Journal of Physical Chemistry B*, 2003, **107**, 5483-5486.
49. L. Jing, B. Xin, F. Yuan, L. Xue, B. Wang and H. Fu, *The Journal of Physical Chemistry B*, 2006, **110**, 17860-17865.
50. S. Sontakke, J MModak and G. Madras, *Chemical Engineering Journal*, 2010, **165**, 225-233.
51. S. Sontakke, C. Mohan, J M Modak and G. Madras, *Chemical Engineering Journal*, 2012, **189–190**, 101-107.
52. A. Benabbou, Z. Derriche, C. Felix, P. Lejeune and C. Guillard, *Applied Catalysis B: Environmental*, 2007, **76**, 257-263.
53. N. K. Eswar, P. C. Ramamurthy and G. Madras, *New Journal of Chemistry*, 2016, **40**, 3464-3475.
54. M. Mittal, M. Sharma and O. P. Pandey, *Solar Energy*, 2014, **110**, 386-397.
55. S. Bai, J. Jiang, Q. Zhang and Y. Xiong, *Chemical Society Reviews*, 2015, **44**, 2893-2939.
56. A.-W. Xu, Y. Gao and H.-Q. Liu, *Journal of Catalysis*, 2002, **207**, 151-157.
57. L. G. Devi and R. Kavitha, *Applied Catalysis B: Environmental*, 2013, **140–141**, 559-587.

Published on 02 September 2016. Downloaded by New York University on 06/09/2016 11:51:34.

RSC Advances Accepted Manuscript

View Article Online
DOI: 10.1039/C6RA16739J

58. R. Mohan, K. Krishnamoorthy and S.-J. Kim, *Solid State Communications*, 2012, **152**, 375-380.
59. C. Wu, L. Shen, H. Yu, Y.-C. Zhang and Q. Huang, *Materials Letters*, 2012, **74**, 236-238.
60. J. Liqiang, Q. Yichun, W. Baiqi, L. Shudan, J. Baojiang, Y. Libin, F. Wei, F. Honggang and S. Jiazhong, *Solar Energy Materials and Solar Cells*, 2006, **90**, 1773-1787.
61. H.-Y. Lin, *Improving the Optoelectronic Property and Photoactivity of Nano-structured Titanuim Dioxide: Effect of Particle Size, Oxygen Vacancy, and Nitrogen Doping*, 2008, Proquest LLC, Michigan, USA.
62. X. Pan, M.-Q. Yang, X. Fu, N. Zhang and Y.-J. Xu, *Nanoscale*, 2013, **5**, 3601-3614.
63. M. Joseph, H. Tabata and T. Kawai, *Japanese Journal of Applied Physics*, 1999, **38**, L1205.
64. T. Yamamoto, *Thin Solid Films*, 2002, **420–421**, 100-106.
65. O. Diwald, T. L. Thompson, T. Zubkov, S. D. Walck and J. T. Yates, *The Journal of Physical Chemistry B*, 2004, **108**, 6004-6008.
66. H. Gan, G. Zhang and H. Huang, *Journal of Hazardous Materials*, 2013, **250–251**, 131-137.
67. S. G. Kumar and L. G. Devi, *The Journal of Physical Chemistry A*, 2011, **115**, 13211-13241.
68. M. I. Litter, *Applied Catalysis B: Environmental*, 1999, **23**, 89-114.
69. A. A. Murashkina, P. D. Murzin, A. V. Rudakova, V. K. Ryabchuk, A. V. Emeline and D. W. Bahnemann, *The Journal of Physical Chemistry C*, 2015, **119**, 24695-24703.

Published on 02 September 2016. Downloaded by New York University on 06/09/2016 11:51:34.

RSC Advances Accepted Manuscript

View Article Online
DOI: 10.1039/C6RA16739J

Visible light driven efficient N and Cu co-doped ZnO for photoinactivation of *Escherichia coli*

Rimzhim Gupta[1], Neerugatti KrishnaRao Eswar[2], Jayant M Modak[1], and Giridhar Madras[1]
[1]Department of Chemical Engineering, [2]Centre for Nanoscience and Engineering, Indian Institute of Science, Bangalore, India

Published on 02 September 2016. Downloaded by New York University on 06/09/2016 11:51:34.

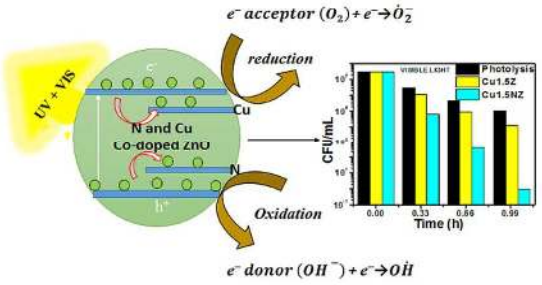

N and Cu co-doped ZnO shows outstanding antibacterial activity for *E.coli* inactivation under visible light

RSC Advances Accepted Manuscript